Heliyon 5 (2019) e02756

Contents lists available at ScienceDirect

Heliyon

journal homepage: www.heliyon.com

Research article

Performance evaluation of surfactant modified kaolin clay in As(III) and As(V) adsorption from groundwater: adsorption kinetics, isotherms and thermodynamics

Rabelani Mudzielwana [a,*], Mugera Wilson Gitari [a], Patrick Ndungu [b]

[a] Environmental Remediation and Nano Science Research Group, Department of Ecology and Resource Management, Thohoyandou, South Africa
[b] Department of Applied Chemistry, University of Johannesburg, South Africa

ARTICLE INFO

Keywords:
Physical chemistry
Thermodynamics
Surfactant
Isotherms
Adsorption
Kinetics
Kaolin clay mineral

ABSTRACT

In this paper surfactant modified kaolin clay for As(III) and As(V) was prepared by intercalating hexadecyltrimethylamonium bromide (HDTMA-Br) cationic surfactant onto the clay interlayers. Batch experiments were used to evaluate the effectiveness of surfactant modified kaolin clay towards As(III) and As(V) removal. The results revealed that adsorption of As(III) and As(V) is optimum at pH range 4–8. The maximum As(III) and As(V) adsorption capacities were found 2.33 and 2.88 mg/g, respectively after 60 min contact time. The data for adsorption of As(III) showed a better fit too pseudo first order model of reaction kinetics while the data for As(V) fitted better to pseudo second order model. The adsorption isotherm data for As(III) and As(V) fitted well to Langmuir model indicating that adsorption of both species occurred on a mono-layered surface. Adsorption thermodynamics model revealed that adsorption of As(III) and As(V) was spontaneous and exothermic. The presence of Mg^{2+} and Ca^{2+} increased As(III) and As(V) adsorption efficiency. The regeneration study showed that synthesized adsorbent can be used for up to 5 times with maximum As(III) and As(V) percentage removal of 54.2% and 62.33%, respectively achieved after 5^{th} cycle. Surfactant modified kaolin clay mineral showed higher adsorption capacity towards As(III) and As(V) as compared to unmodified kaolin clay mineral and competitive with other adsorbent in the literature. The results obtained from this study revealed that surfactant modified kaolin mineral is a candidate material for arsenic remediation from groundwater.

1. Introduction

Groundwater is the common source of water in majority of rural areas particularly in arid and semi-arid regions where surface water resources and rainfall are scarce. However, groundwater often contain toxic elements such as arsenic. In groundwater, arsenic exist as oxyanions of trivalent arsenite [As(III)] under oxidizing conditions and pentavalent arsenate [As(V)] under reducing conditions (Smedley and Kinniburgh, 2002). The prolonged exposure to groundwater containing higher concentrations of inorganic arsenic is linked to different types of cancer, neurological diseases and cardiovascular diseases (Smith and Smith, 2004; Sarkar and Paul, 2016).

The World Health Organization (WHO) has estimated that at least 140 million people in more than 50 counties worldwide relies on water containing arsenic concentrations above the permissible limits of 10 μg/L (World Health Organization, 2011). The worst affected countries includes Bangladesh, India, Argentina, Mexico, and China. In Africa, the estimate of people exposed to higher concentration of arsenic is unknown. However, higher concentrations of arsenic has been reported in countries like South Africa, Burkina Faso, Ghana and Zimbabwe (Kempster et al., 2007; Fatoki et al., 2013; Bretzler et al., 2017). Owing to toxicity of arsenic efforts towards removal of arsenic from groundwater to a permissible levels for drinking purposes are being encouraged.

So far, several techniques including oxidation (McCann et al., 2018), coagulation and precipitation (Cui et al., 2015), adsorption (Ren et al., 2014), ion exchange (Pakzadeh and Batista, 2011) and membrane techniques (Kang et al., 2000) have been developed and tested for their efficiency in arsenic removal. However, most of these techniques are expensive, generates toxic sludge and requires skilled labor for operation (Sarkar and Paul, 2016). Adsorption technique appears to be the suitable method that can be applied for arsenic removal particularly in rural areas because it uses materials that are found at little or no costs such as clay

* Corresponding author.
E-mail addresses: mudzrabe@gmail.com, 11600806@mvula.univen.ac.za (R. Mudzielwana).

https://doi.org/10.1016/j.heliyon.2019.e02756
Received 27 March 2019; Received in revised form 20 May 2019; Accepted 28 October 2019

minerals (Bentahar et al., 2016), activated carbon (Arcibar-Orozco et al., 2014), activated alumina, bone char (Saikia et al., 2017), macrofungus biomass (Sari and Tuzen, 2009) and coal fly ash (Wang et al., 2008).

Clay is a natural, earthy, fine grained material mainly composed of crystalline minerals. Over the years clays have been used for industrial purposes as well as in the adsorption or organic and inorganic substances from water (Tuzen et al., 2006). Their use in adsorption of contaminants is mainly attributed to their strong adsorptive properties such as larger surface area, higher cation exchange capacity and chemical and mechanical stability. Furthermore, clays can be modified to enhance their sorption capacity. Synthesis of organically modified clay minerals for arsenic removal has recently received great attention from researchers. Organoclays are prepared through intercalation of cationic surfactant onto the interlayers of the clay minerals. This is achieved through ionic exchange between Na^{+}, Ca^{2+}, K^{+} and Mg^{2+} in the clay interlayers and the cationic surfactant where the net surface charges of the clay are reversed from negative to positive (Su et al., 2011). This modification enhances the sorption of anions via ion exchange (Reeve and Fallowfield, 2018). Su et al. (2011) prepared a surfactant modified bentonite clay for As(V) and As(III) removal from aqueous solution and reported maximum adsorption capacity of 0.28 and 0.10 mg/g for As(V) and As(III), respectively. The achieved results showed improved adsorption capacity compared to those achieved from unmodified bentonite under the same experimental conditions. Chutia et al. (2009) also reported an improved sorption capacity of hexadecyltrimethylamonium bromide (HDTMA) modified mordenite and clinoptilolite clay minerals for As(V) as compared to unmodified ones. Nevertheless, little has been done on the modification of kaolin clay mineral using cationic surfactant for As(III)/As(V) removal. This study aims at preparing a surfactant modified kaolin clay mineral for simultaneous As(III) and As(V) removal from groundwater. Batch experiments were used to evaluate the effects of contact time and adsorption isotherm, effect of adsorbate concentration and adsorption isotherms and thermodynamics, effect of pH and co-existing ions. Furthermore, the regeneration and reuse of adsorbent were evaluated.

2. Material and methods

2.1. Materials

Natural kaolin clay mineral was collected from Dzamba Village in Limpopo Province, South Africa. Hexadecyltriammonium bromide (HDTMA-Br) was purchased from Merk chemicals, South Africa. Other analytical grade reagents including $HAsNa_2O_4.7H_2O$ and $AsNaO_2$ were purchased from Rochelle Chemicals, South Africa.

2.2. Synthesis of surfactant modified kaolin clay (SMK)

Prior to modification the clay was washed using Milli-Q water at a mass/volume ratio of 1:5 to remove suspended organic matter. Clay sample was then oven dried at 105 °C for 12 h. Dried clay was then pulverized using a mortar and pestle to pass through 250μm sieve. To synthesize surfactant modified kaolin clay (SMK), a solution containing 5 mM of HDTMA-Br was prepared by dissolving appropriate amount of HDTMA-Br in 1000 mL volumetric flask using Milli-Q water. Thereafter, 100 mL of the solution was pipetted onto 250 mL plastic bottle and 1 g of raw kaolin clay (RK) to make up an S/L ratio of 1 g/100 mL. Mixture was agitated for 60 min on a Table shaker. After agitation, mixtures were filtered through 0.45 μm membrane filters. Residues were washed with Milli-Q water several times to remove excess surfactant. Obtained residues were then oven dried at 60 °C for 12 h and then pulverized using mortar and pestle to pass through 250 μm sieve. The experiment was repeated until adequate adsorbent was synthesized.

2.3. Characterization of the material

PANalytical X'Pert Pro powder X-ray diffractometer (XRD) (Bruker, Germany) and S1 Titan X-ray fluorescence (XRF) (Bruker, Germany) techniques were employed to examine the mineralogical and elemental composition of the clay respectively. Infra-red spectrum of the adsorbent was obtained using Fourier Transform Infra-red spectrum equipped with ATR-Diamond (Bruker, Germany). Morphological characteristics were determined using scanning electron microscopy (SEM) (Leo1450 SEM, voltage 10 kV, working distance 14 mm). The pore size distribution, pore volume and pore diameter were determined by Barrett Joyner Halenda (BJH) sorption model using a specific surface area analyzer (Autosorb-iQ & Quadrasorb SI, USA). Nitrogen adsorption-desorption isotherms were used to determine specific surface area of the adsorbent according to Brunauer Emmett Teller (BET) model. The pHpzc of the clay was determined using titration method as described by Gitari et al. (2015).

2.4. Batch adsorption

Stock solutions containing 1000 mg/L As(III) and As(V) were prepared by dissolving 0.1733 g of $AsNaO_2$ and 0.416 g of $HAsNa2O_4.7H_2O$, respectively in 100 mL volumetric flask using Milli-Q water (18.2 MΩ/cm). The working solutions were prepared through appropriate dilutions from the stock solution. To evaluate the effect of contact time and adsorption kinetics, contact time was varied from 10 to 120 min. Adsorbent dosage of 0.15 g/100 mL and adsorbate concentration of 5 mg/L were maintained. After agitation, mixtures were centrifuged at 2 500 rpm for 10 min. The optimum adsorbent dosage was evaluated by varying adsorbent dosage from 0.05-0.5 g/100 mL. Contact time of 60 min and adsorbate concentration of 5 mg/L were maintained. To evaluate the adsorbate concentration and adsorption isotherms, initial concentration of As(III)/As(V) was varied from 1 to 30 mg/L and adsorbent dosage of 0.4 g/100 mL, contact time of 60 min were maintained. The experiment was conducted at a temperature of 298, 323 and 343 K. The obtained data was used to evaluate the adsorption thermodynamics. The effect of initial pH was evaluated at initial adsorbate concentration of 5 mg/L, contact time of 60 min and adsorbent dosage of 0.4 g/100 mL. The initial pH was adjusted from 2-12 using 0.01 M NaOH and 0.01 M HCl. The influence of co-existing ions (F^{-}, Cl^{-}, NO_3^{-}, CO_3^{2-}, SO_4^{2-}, Mg^{2+} and Ca^{2+}) was evaluated at the initial concentration As(III)/As(V) concentration of 3 mg/L, adsorbent dosage of 0.4 g/100 mL, 60 min contact time. The initial concentration of each co-existing ion was 5 mg/L. All experiments were conducted in triplicate and the mean values were reported. Unless otherwise stated, experiments were conducted at room temperature and initial pH of 6 ± 0.5.

2.5. Desorption and reuse of the adsorbent

To evaluate the regeneration and reuse potential of the adsorbent: As(III)/As(V) removal experiment was conducted by treating solution containing 5 mg/L As(III)/As(V) with 1.0 g of SMK at initial pH of 6 ± 0.5 for 60 min. After agitation, mixtures were filtered through 0.45 μm filter membranes. Residues were washed with Milli-Q water and oven dried for 12 h at 60 °C. The obtained residues were pulverized with a mortar and pestle to pass through 250 μm sieve, weighed and then regenerated using 100 mL of 0.01 M Na_2CO_3 by agitating the mixture for 60 min. After regeneration, the adsorbent was reused for As(III)/As(V) removal experiment. The regeneration-reuse cycle were continued up to 5^{th} cycle.

2.6. Column experiments

Column tests were carried using a plastic column with the internal diameter of 2.5 cm and a total length of 13.5 cm. 5 g of the adsorbent was packed in the column to make a bed height of 1.2 cm. Groundwater collected from Siloam community borehole was spiked with arsenic solution to get desired total arsenic concentration of 0.5 and 1.5 mg/L and

used as a feed water. The feed water was passed through the column in an up-flow mode using a Gilson peristaltic pump at a flow rate of 1.5 mL/min. The effluents were collected at a regular interval and analyzed for total arsenic concentration. Fig. 1 present the set-up for column experiment.

2.7. Analysis of residual arsenic

The residual As(III)/As(V) concentration was measured using ScTRACE Gold electrode attached to 884 professional VA Polarography (Metrohm, SA). A composite solution containing 1 mol/L sulfamic acid, 0.5 mol/L citric acid and 0.45 mol/L KCl was used an electrolyte. For total As concentration, $KMnO_4$ was added as an oxidizing agent. For quality control, samples were also analyzed using metrohm 850 professional ion chromatography (Switzerland) for As(III) and As(V) concentration. Metrosep A Supp 5–150 column was used for separation and the guard column Metrosep A 4/5 was used. The eluent containing 15 mmol/L NaOH and 2.0 mmol/L Na_2CO_3 was used as the mobile phase. The concentration of As(III) was determined without suppression. The conductivity detector was used to estimate the concentration of different chemical species. Total arsenic concentration was determined using ICP-MS.

3. Results and discussion

3.1. Mineralogical analysis

Fig. 2 presents the XRD pattern of raw kaolin (RK) and surfactant modified kaolin (SMK) clay. The results showed that the clay is mainly consist of quartz and kaolin as the main minerals. No change observed in the XRD pattern of the kaolin clay after modification with HDTMA-Br. This could be indicating that sorption of HDTMA-Br onto the surface of kaolin clay mineral did not affect the clay interlayers. The same observation was reported by Sun et al. (2017) during modification of illite clay using CTAB.

3.2. Chemical composition

Table 1 presents the elemental composition of raw and modified kaolin mineral determined using XRF. The results showed that SiO_2 and Al_2O_3 are the main constituents of the clay mineral averaging 57.1 and 22.05%, respectively followed by Fe_2O_3 averaging 3.88%. These results confirms that this clay is an alumino-silicate material. After modification the content of SiO_2, Al_2O_3 and Fe_2O_3 decreased to 51.97, 18.79 and 2.85 %, respectively. This could be attributed to their dilution during intercalation of cationic surfactant interlayers. The content of exchangeable oxides such as MgO, CaO and K_2O decreased after modification (Table 1). This suggest that the modification involves ion exchange reaction between Mg^{2+}, K^+ and Ca^{2+} and the surfactant.

3.3. FTIR analysis

The FTIR spectrums of RK, HDTMA-Br, SMK before and after arsenic removal are presented in Fig. 3. For RK, the absorption bands at 3698.54 and 1695.25 cm^{-1} are ascribed to –OH stretching vibration in physiosorbed water. Bands at 1003.68 and 964.92 cm^{-1} are attributed to the vibration of Si–OH and Al–OH bonds, respectively. The bands at lower wavelength are ascribed to the vibration of Al–O–Si and Si–O–Si networks. The HDTMA-Br spectrum showed a stronger absorption bands at the region of 2849.72 and 2917.03 cm^{-1} which are assigned to the C–H stretching bond of the $–CH_3$ and $–CH_2$ groups. The band at 1462.59 cm^{-1} is attributed to the vibration of C–C–C flexural vibration associated with methylene groups. The bands at 911.82 cm^{-1} and 966.9 cm^{-1} are associated with the vibration and stretching of C–N bonds. The successful modification of the kaolin clay is confirmed by the bands at 2858.13 and 2923.41 cm^{-1} which are ascribed to the vibration of C–H bonds which were observed after modification. After arsenic removal, no change was observed in the spectrum of the modified clay. However, there was an increase in the transmittance intensity of the bands. This could be an indication that adsorption of arsenic could be through surface complexation.

3.4. Surface morphology

The SEM micrographs of RK and SMK before and after arsenic adsorption together with their respective EDX spectrum are presented in Figure 4A-F. The analysis revealed that RK has a spongy like morphology with different sized agglomerates of fine particles (Fig. 4A). No significant change can be observed on the surface of the clay after modification (Fig. 4C). However, the surface seemed covered with small particles, suggesting a better adhesion of small particles onto the larger ones. This could be attributed to change in the surface hydrophobicity and thus free adhesion (Sun et al., 2017). After arsenic adsorption, more agglomerates of irregular sizes and shapes are observed on the surface of the adsorbent (Fig. 4E). The SEM-EDX spectrum confirmed the presence of exchangeable cations such as K^+, Mg^{2+} and Ca^{2+} in RK (Fig. 4B) clay and the absence of these cations in the SMK spectrum (Fig. 4D). This results are complimented by the XRF results (Table 1) which showed the decrease in

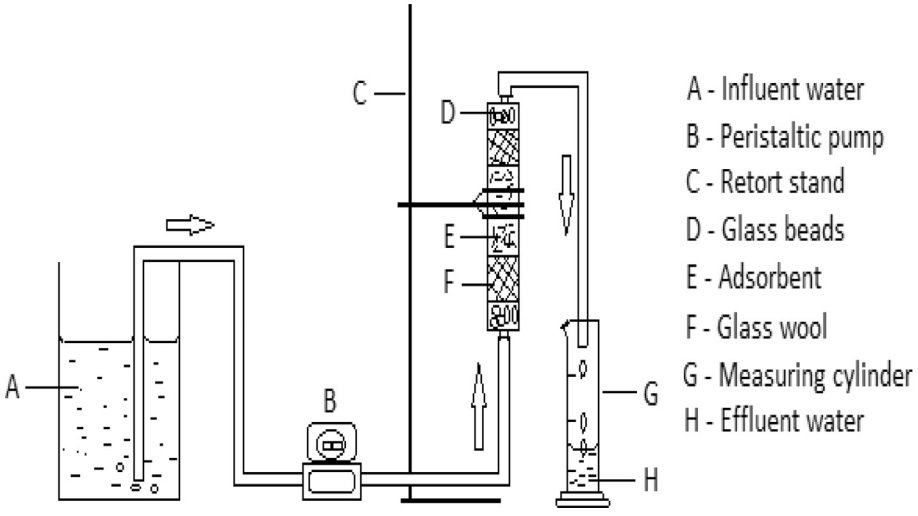

Fig. 1. Experimental set-up for column experiments.

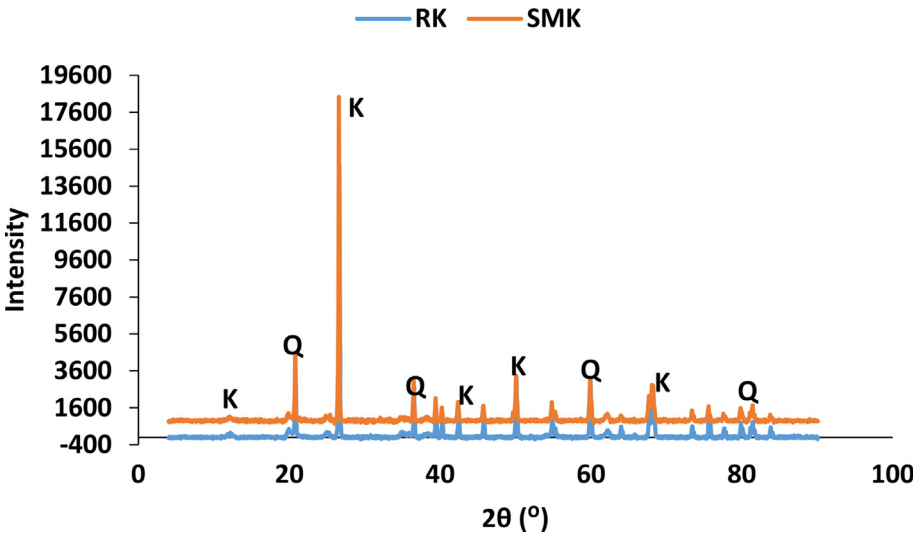

Fig. 2. X-ray diffraction patterns of RK and SMK (Q- Quartz, K-Kaolin).

Table 1
Elemental composition of RK and SMK.

Oxides	RK (%w/w)	SMK (%w/w)
SiO_2	57.1	51.67
Al_2O_3	22.05	18.79
Fe_2O_3	3.88	2.85
MgO	0.57	<LOD*
MnO	0.02	0.02
CaO	0.95	0.39
K_2O	0.16	0.01
TiO_2	1.76	1.0
P_2O_5	0.02	0.041

*LOD: Limit of Detection.

percentage weight of MgO, CaO and K_2O oxides. No Ca^{2+} ions may be observed on the EDX spectrum of the clay after arsenic adsorption which suggests that Ca^{2+} ions were exchanged during arsenic adsorption.

3.5. Surface area analysis

Table 2 present the BET surface area, pore volume and pore diameter of RK and SMK. The analysis revealed that the total surface area of kaolin clay mineral decreased drastically from 18.61 to 3.39 m^2/g after modification with the cationic surfactant. Conversely, the pore volume and the pore diameter increased from 0.04 to 0.07 cc/g and 9.53–20.41 nm, respectively. This results are similar to the ones reported by Zhu and Zhu (2007) and Lee et al. (2015) for surfactant modified clays. The decrease in surface area and the increase in pore volume and pore diameter is attributed to the fact that intercalated surfactant filled up most of the gallery space in the clay surface resulting in propping up of the interlayer leading to increased pore volume and pore diameter. Based on the average pore diameter (20.41 nm) it is concluded that the synthesized material is mesoporous.

3.6. pH point of zero charge (pHpzc)

Fig. 5 presents the pHpzc of the raw kaolin clay mineral and the surfactant modified clay mineral. The results showed that modification of kaolin clay mineral increased the pHpzc of the clay from 6.5 to 7.5. The pHpzc represent the pH at which the net surface charge of the clay will be zero. At pH above the pHpzc the clay will be negatively charged while at pH below the pHpzc the clay will be positively charged (Gitari et al.,

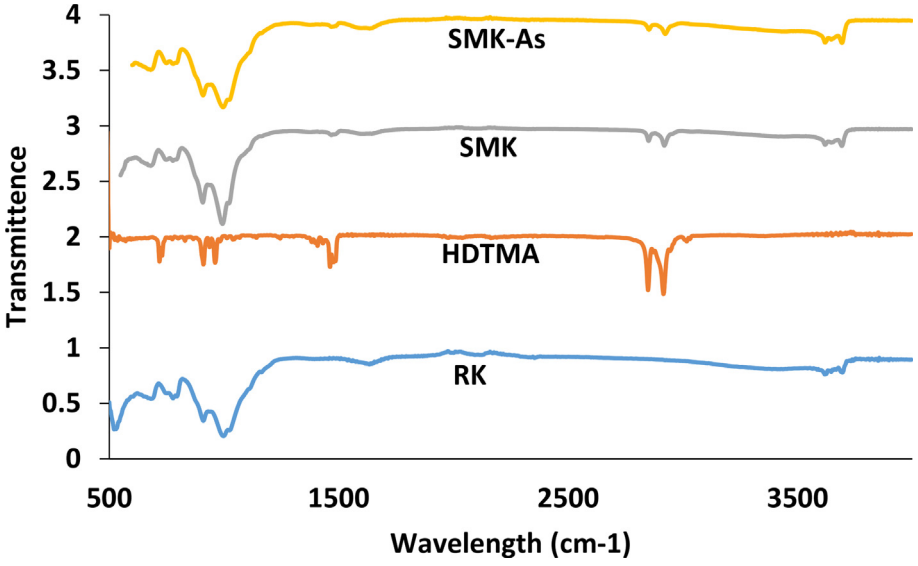

Fig. 3. FTIR spectrum of RK, HDTMA and SMK before and after As removal.

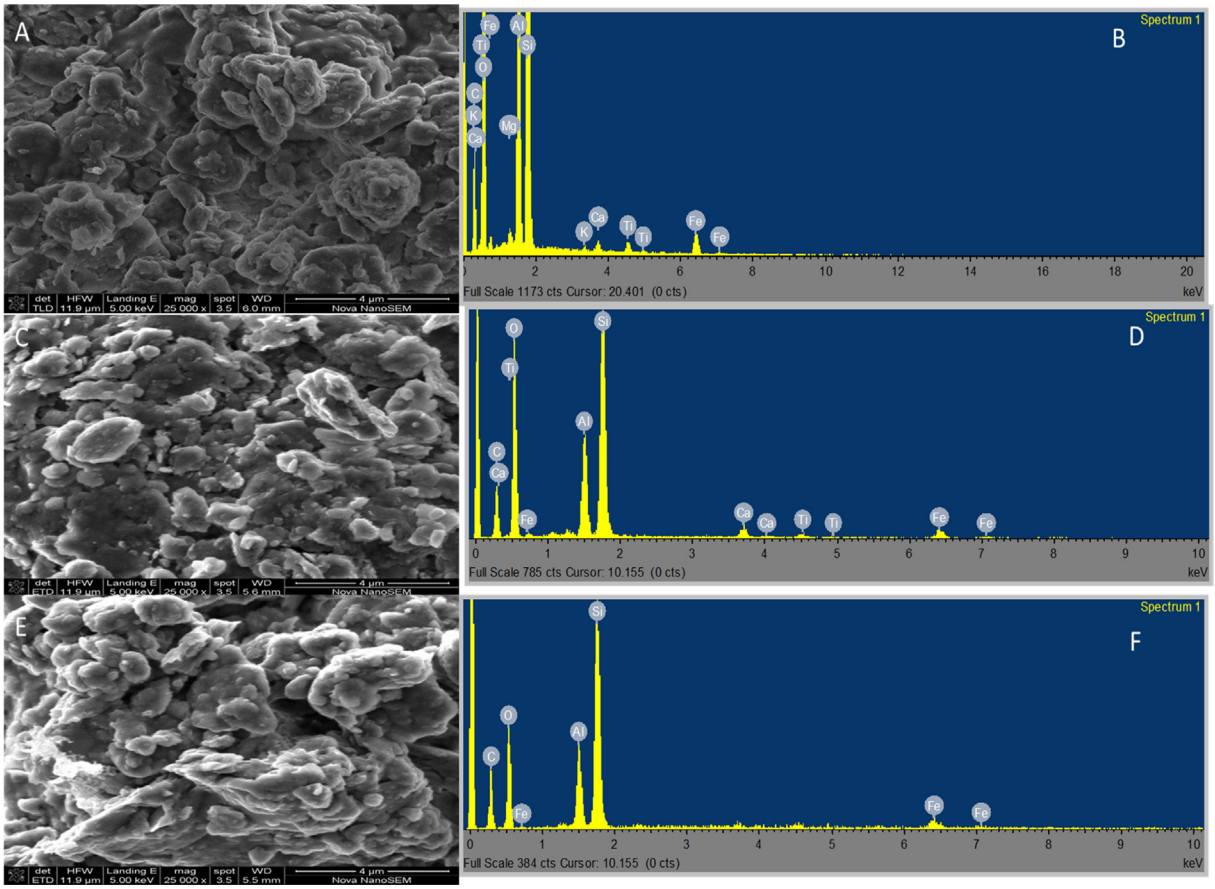

Fig. 4. SEM micrographs and EDX spectrums of RK (A and B) and SMK before (C and D) and after arsenic adsorption (E–F).

Table 2
Surface area, pore volume and pore diameter of RK and SMK.

	BET surface area (m^2/g)	Pore volume (cc/g)	Pore diameter (nm)
RK	18.61	0.04	9.53
SMK	3.39	0.07	20.41

2015). The increase in pHpzc after modification indicates that modification of the clay by HDTMA enhanced the net positive charges of the clay mineral. This could enhance the pH range at which the adsorption of arsenic oxyanions will be optimum.

3.7. *Effect of contact time and adsorption kinetics*

Fig. 6 shows the effect of contact time on percentage As(III) and As(V) removal by SMK. It is observed that the percentage of removal for As(III) and As(V) was rapid within the first 60 min of contact time and relatively slower at contact time beyond 60 min which indicate that the adsorbent surface is saturated and the system has reached equilibrium. The rapid adsorption at contact time below 60 min could be attributed to large number of available active sorption sites for As(III) and As(V) on the surface of the adsorbent. Therefore, 60 min was chosen to be the optimum contact time for further experiments.

Examination of reaction kinetics is one of the important factor in the design of adsorption system (Saleh et al., 2016). In order to determine the efficiency of the adsorption processes and to provide insight of the As(III) and As(V) adsorption mechanism as well as the rate limiting steps, the commonly used pseudo-first-order (PFO) and pseudo-second-order (PSO) reaction kinetics models together with the intra-particle diffusion model of Webber-Morris were applied to fit the experimental data (Gupta and Bhattachryya, 2011; Tran et al., 2017). Pseudo-first-order and

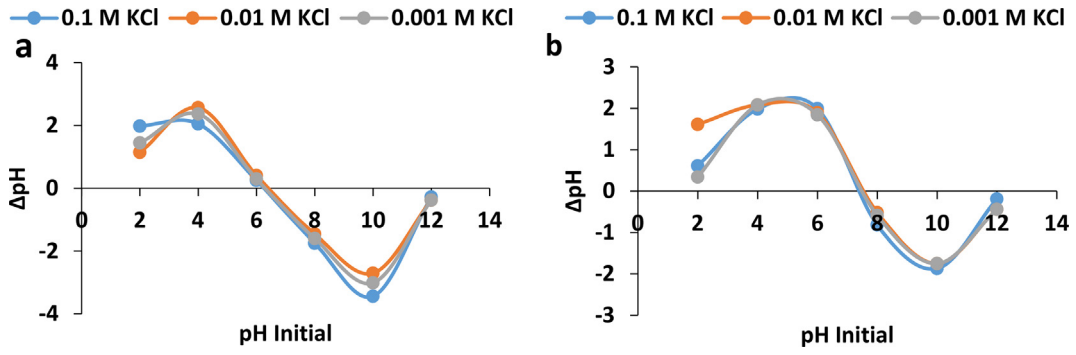

Fig. 5. pHpzc of RK (a) and SMK (b).

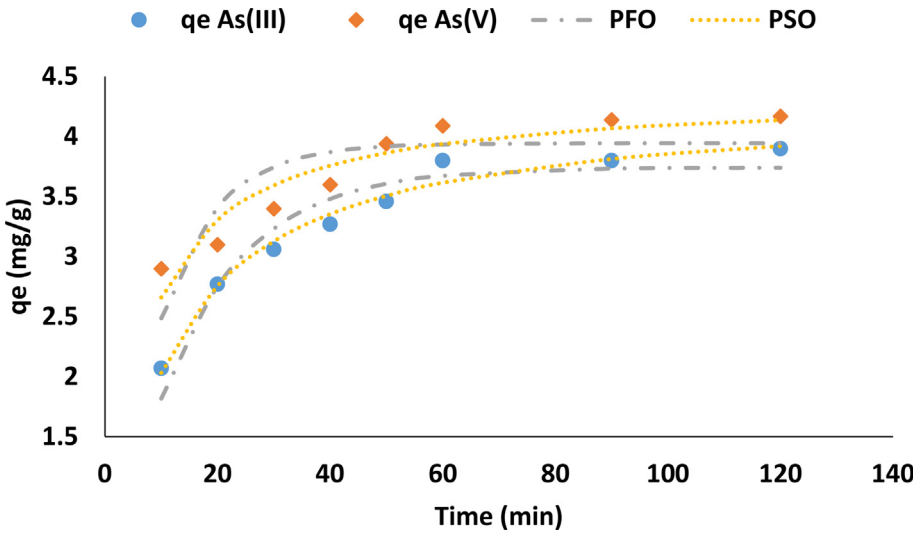

Fig. 6. Adsorption kinetics for As(III) and As(V) onto SMK (initial concentration of 5 mg/L, adsorbent dosage of 0.1 g/100 mL, pH 6).

pseudo-second-order reaction models are expressed by Eqs. (1) and (2) while Eq. (3) expresses the intra-particle diffusion model (Ho et al., 1996; Ho, 2004; Weber and Morris, 1963).

$$q_t = q_e(1 - e^{-k_1 t}) \quad (1)$$

$$q_t = \frac{q_e^2 k_2 t}{1 + k_2 q_e t} \quad (2)$$

$$q_t = k_i t^{0.5} + C \quad (3)$$

where q_e (mg/g) and q_t (mg/g) represent the adsorption capacity at equilibrium and at time t (min), respectively; k_1 (min^{-1}), k_2 (g/mg.min), k_i ($mg/g.min^{-0.5}$) are rate constants for PFO, PSO and intra-particle diffusion model, respectively and C, intercept is the constant associated to the thickness of the boundary layer. Higher value of C correspond to the greater effect on the limiting boundary layer. The nonlinear plots for PFO and PSO kinetics models for As(III) and As(V) adsorption are presented in Fig. 6. The PFO and PSO parameters estimated by nonlinear regression are presented in Table 3.

Based on the correlation coefficient (R^2) and the model adsorption capacity values, the adsorption of As(III) was described better by PFO while the data for As(V) was described better by PSO. This indicate that adsorption of As(III) onto SMK occurred via physiosorption whereas the adsorption of As(V) occurred through chemisorption. The intra-particle plot presented in Fig. 7 exhibited two clearly defined phases which indicates the possibility of external surface adsorption on the macro-pores (phase 1) and intra-particle diffusion into micro-pores and mesopores of the adsorbent (phase 2). At phase 1 arsenic ions are attracted physically to the surface while at phase 2 arsenic ions are adsorbed through ion exchanges between the hydroxyl ions and arsenic ions within the particles. The model constant are as presented in Table 4 shows that the K_{i1} values are higher than the k_{i2} values indicating that the external surface adsorption was much faster than the intra-particle diffusion. The intra-particle diffusion in phase 2 was confirmed by higher C_2 value which is an indication of thicker boundary (Table 4).

Table 3
Constant parameters for pseudo-first-order and pseudo-second-order models of reaction kinetics.

	PFO	K_1 (min^{-1})	R^2	PSO	K_2 (g/mg.min)	R^2
	q_e (mg/g)			q_e (mg/g)		
As(III)	3.7	0.1	0.92	2.1	0.27	0.88
As(V)	3.99	0.09	0.66	4.35	0.03	0.98

3.8. Effect of adsorbent dosage

Fig. 8 depicts the effect of adsorbent dosage onto As(III) and As(V) adsorption by SMK. It is observed that the removal efficiency of As(III) and As(V) increased with increasing adsorbent dosage from 0.05 g/100 mL to 0.2 g/100 mL where it reached the plateau. The adsorption efficiency remained almost constant at dosage beyond 0.2 g/100 mL indicating that the adsorbent has reached its maximum sorption capacity. The increase in removal efficiency with adsorbent dosage could be attributed to increasing number of active sites available for As(III) and As(V) sorption. For subsequent experiments, 0.4 g/100 mL adsorbent dosage was used in order to ensure optimum uptake of As(III) and As(V) species.

3.9. Adsorption isotherms

To evaluate As(III) and As(V) adsorption isotherms, the initial concentration was varied from 1 to 30 mg/L and the experiment was repeated at a temperature of 298, 323 and 343 K. The results are presented in Fig. 9. It is observed that As(III) and As(V) adsorption capacities increase with increasing equilibrium concentration. The same trend was observed at both temperatures. In order to describe the relationship between the adsorbate concentration and adsorbent, the non-linear equations of Langmuir (Eq. 4) and Freundlich (Eq. 5) adsorption isotherm models were used to describe the data (Firdaous et al., 2017).

$$q_e = \frac{q_{max} b C_e}{1 + b C_e} \quad (4)$$

$$q_e = K_f C_e^{1/n} \quad (5)$$

where q_e (mg/g) is the adsorption capacity, C_e (mg/L) is the As(III) and As(V) concentration at equilibrium, b (L/mg) is the equilibrium adsorption constant related to the affinity of the binding sites, q_{max} (mg/g) is the maximum monolayer adsorption capacity of the adsorbent. The higher the b and q_{max} values the better the adsorbent (Tran et al., 2017). K_f (mg/g) is the Freundlich constant related to adsorption capacity and 1/n is the dimensionless parameter for Freundlich adsorption isotherm model related to adsorption intensity which indicates the magnitude of the adsorption driving force or surface heterogeneity. Adsorption is favorable when $1/n < 1$, unfavorable when $1/n > 1$, linear when $1/n = 1$ and irreversible when $1/n = 0$. Langmuir and Freundlich adsorption

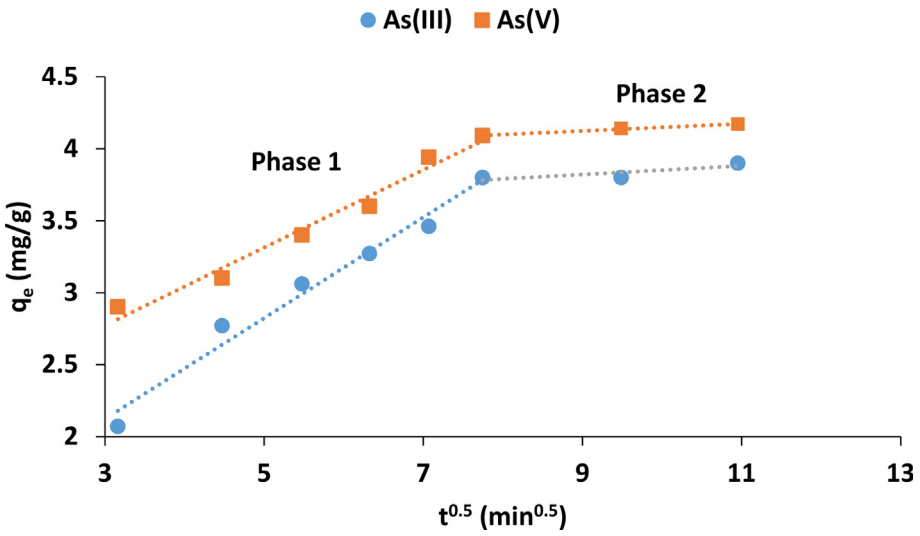

Fig. 7. Intra-particle diffusion model for As(III) and As(V) adsorption onto SMK.

Table 4
Constant parameters for intra-particle diffusion model.

	K_{i1} (mg/g.$min^{-0.5}$)	C_1	K_{i2} (mg/g.$min^{-0.5}$)	C_2
As(III)	0.35	1.07	0.03	3.54
As(V)	0.27	1.96	0.02	3.89

isotherm nonlinear fitting curves for As(III) and As(V) adsorption by SMK are presented in Fig. 9 and the models constant values are presented in Table 5.

Based on the regression co-efficient value, the adsorption data fitted better to Langmuir adsorption isotherm model. This suggests that adsorption of As(III) and As(V) occurred on a mono-layered surface of SMK. Once the adsorbate molecule occupies a site, no further adsorption can take place on that site (Al-Othman and Naushad, 2012; Hong et al., 2004). The maximum adsorption capacity for Langmuir adsorption isotherm model (q_{max}) was observed to be decreasing with increasing temperature. The results showed that SMK has a stronger affinity towards As(V) as compared to As(III). The essential characteristics of the Langmuir isotherm model can be expressed by the dimensionless constant which is also called a separation factor or equilibrium parameter, R_L which is expressed by Eq. (6) (Tran et al., 2017).

$$R_L = \frac{1}{1 + bC_0} \tag{6}$$

where R_L is the dimensionless separation factor, C_o is the initial As(III) and As(V) concentration and b (L/mg). Adsorption is favorable when R_L <1, unfavorable when R_L>1, linear when R_L = 0 and when R_L = 1 adsorption is irreversible. The calculated R_L values for adsorption of As(III) and As(V) are presented in Figure 10a and b. It is observed that R_L values for both arsenic species lies between 0 and l indicating that was favorable. This findings are in good agreement with the 1/n value obtained from Freundlich adsorption isotherm (Table 5) which also suggested that adsorption was favorable.

3.10. Adsorption thermodynamics

In order to confirm the As(III)/As(V) adsorption mechanism, the adsorption thermodynamic parameters (ΔG°, ΔH° and ΔS°) were determined from the Gibbs free energy equation (Eq. 7) (Tran et al., 2016).

$$\Delta G^\circ = \Delta H^\circ - T\Delta S^\circ \tag{7}$$

where ΔG° is the Gibbs free energy change constant, ΔH° is the standard enthalpy change while ΔS° is the standard entropy change. For every spontaneous sorption process, ΔG° value must be negative (Lonappan

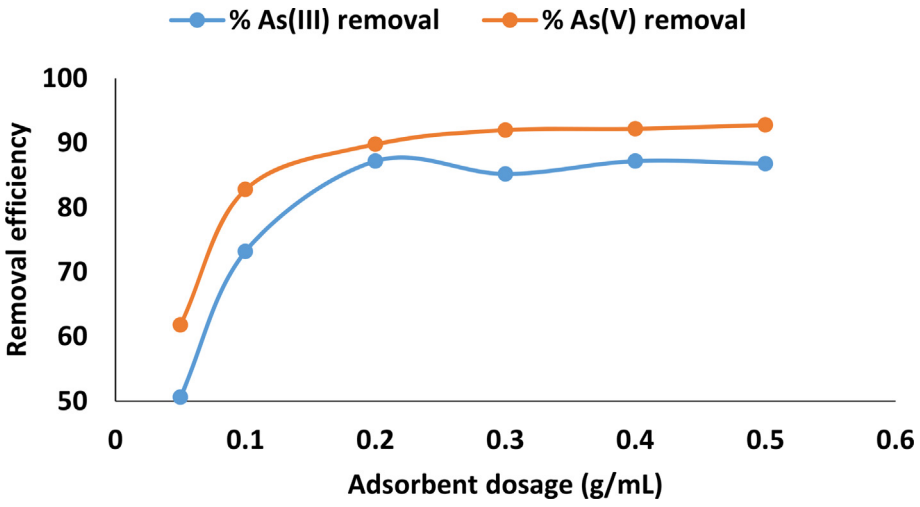

Fig. 8. Effect of adsorbent dosage on As(III) and As(V) removal (Adsorbate concentration: 5 mg/L; contact time: 60 min; shaking speed: 250 rpm; pH 6 ± 0.5).

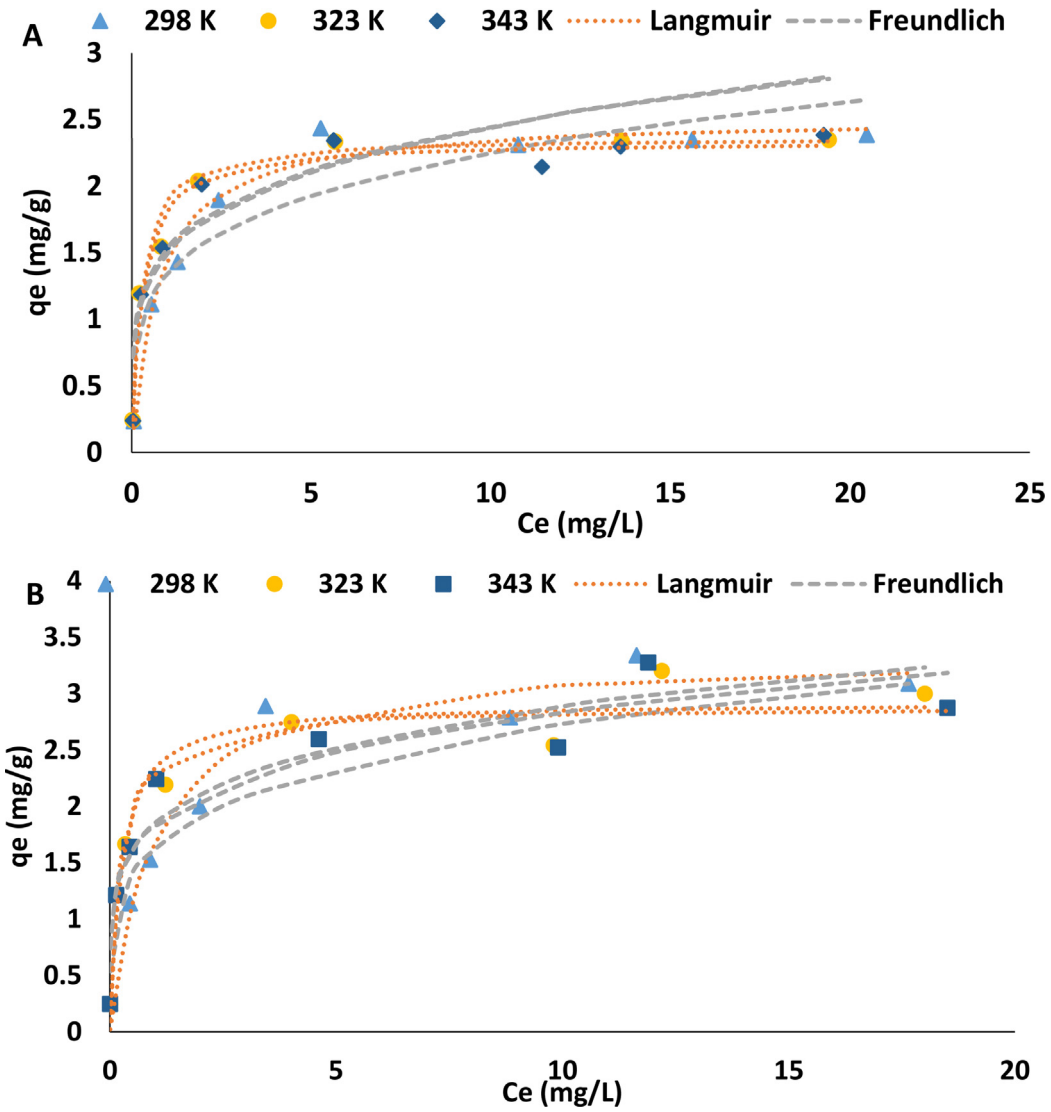

Fig. 9. Adsorption isotherms for As(III) (a) and As(V) (b) adsorption onto SMK (adsorbent dosage: 0.4 g/100 mL, pH: 6 ± 0.5, contact time: 60 min and shaking speed: 250 rpm).

Table 5
Adsorption isotherm parameters for As(III) and As(V) adsorption onto SMK.

		Langmuir			Freundlich		
		q_{max} (mg/g)	B (L/mg)	R^2	K_f (mg/g)	1/n	R^2
As(III)	298 K	2.51	1.32	0.97	1.34	0.22	0.85
	323 K	2.37	3.71	0.97	1.54	0.2	0.88
	343 K	2.33	3.27	0.97	1.48	0.21	0.88
As(V)	298 K	3.36	1	0.96	1.62	0.22	0.86
	323 K	2.9	3.98	0.95	1.84	0.19	0.90
	343 K	2.88	3.72	0.94	1.82	0.19	0.88

et al., 2018).

In sorption equilibria, the equilibrium constant, K_L which is the Langmuir constant is related to Gibbs free energy change by the Eq. (8) (Gitari et al., 2017):

$$\Delta G^{\circ} = -RT \ln K_L \tag{8}$$

where R is the molar gas constant, 8.314 J $mol^{-1}K^{-1}$, T is the absolute temperature in Kelvin.

Eq. (9) is obtained by substituting Eq. .

$$\ln K_L = -\frac{\Delta H^{\circ}}{RT} + \frac{\Delta S^{\circ}}{R} \tag{9}$$

The Gibbs free energy change (ΔG°) is directly calculated from Eq. (7), while the change in enthalpy (ΔH°) and the change in entropy (ΔS°) are determined from the slope and intercept of a plot of $\ln K_L$ against 1/T (Fig. 11). Thermodynamic parameter are presented in Table 6 below. The negative value of ΔG° suggest that the adsorption of As(III) and As(V) was spontaneous. The positive value of ΔS° suggests that As(III)/As(V) ions were randomly distributed on the surface of the adsorbent during adsorption process and the adsorbent has a good affinity towards As(III) and As(V) (Naushad et al., 2017; Lin et al., 2017). The negative ΔH° value indicates that the adsorption of As(III) and As(V) was exothermic reaction. This means the reaction for adsorption of As(III) and As(V) releases heat energy to its surroundings (Tran et al., 2016). Exothermic reactions involves both physiosoprtion and chemisorption adsorption processes. This indicates strong interaction between As(III)/As(V) and the adsorbent sites.

3.11. *Effect of initial pH*

The effect of pH on As(III) and As(V) adsorption is presented in

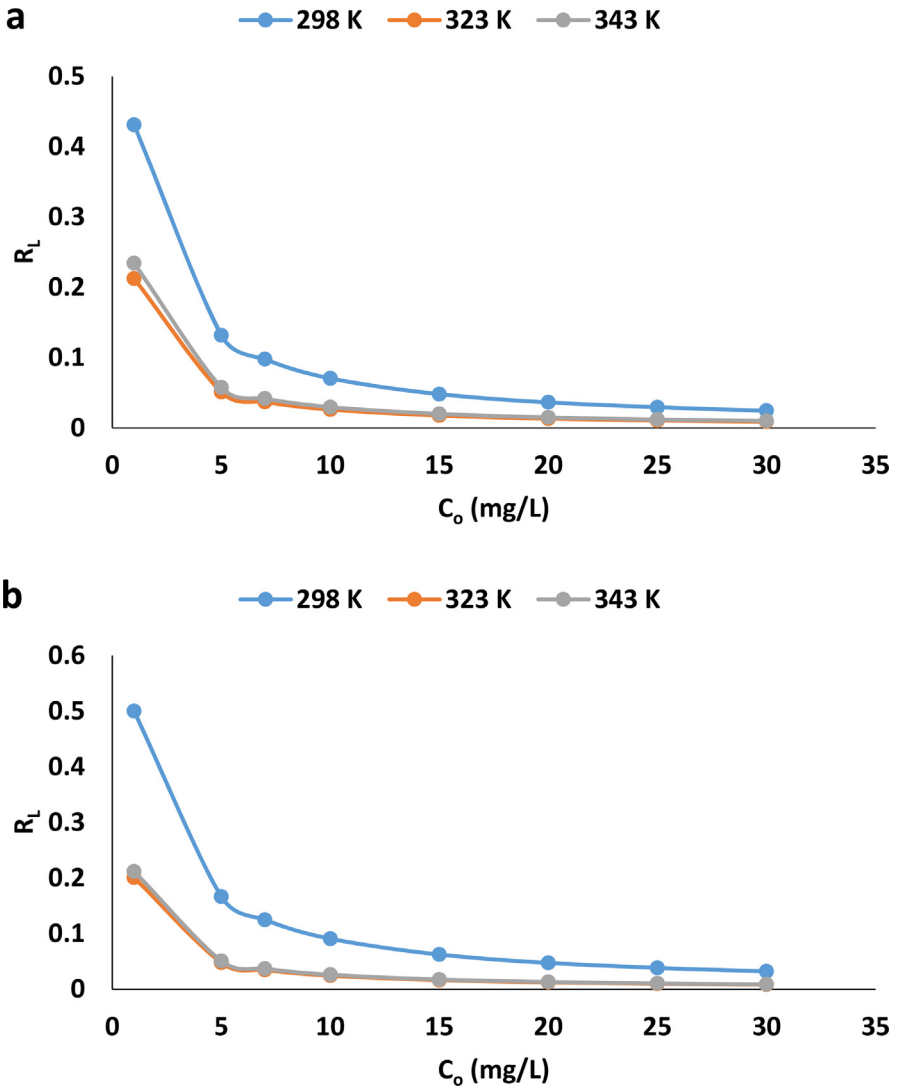

Fig. 10. Values for separation factor, R_L for the adsorption of As(III) (a) As(V) (b).

Fig. 12. It is observed that the removal of As(III) and As(V) was optimum at moderate pH range (pH = 4–8). However, the removal was negligible at extreme acidic and alkaline conditions. The behavior of As(III) and As(V) at various pH levels can be explained based on the arsenic speciation and also the overall surface charges of the adsorbent. The pH point of zero charge (pHpzc) of the SMK evaluated using titration was found to be ≈ 7.5. Therefore, below this pH the adsorbent is positively charged and above this pH the adsorbent is negatively charged. The speciation of As(III) carried out using Visual MINTEQ 3.1 version has revealed that at pH below 8, As(III) exist as neutrally charged H_3AsO_3 and beyond this pH the negatively charged species $H_2AsO_3^-$, $HAsO_3^{2-}$ and AsO_3^{3-} dominate the solution. This findings corroborated by the observations reported by Lee et al. (2015). Low uptake of As(III) at lower pH where H^+ dominate the surface of the adsorbent could be attributed to suppressed deprotonating of neutrally charged H_3AsO_3 (Eq. 10) (Bhowmick et al., 2014). At moderate pH there is low charge density on the surface of the adsorbent which facilitate the Van der Waal attractive forces resulting in optimum uptake of As(III) (Eq. 10). Furthermore, at extreme alkaline pH levels both the surface and As(III) possess negative charges resulting in strong repulsive forces and consequently low As(III) uptake (Eqs. (12) and (13)) (Lee et al., 2015).

$$\equiv S - OH_2^+ + H_3AsO_3 \rightarrow \equiv S - OH - H_2AsO_3 + H_2O \quad (10)$$

$$\equiv S - OH_2^+ + H_2As_3^- \rightarrow \equiv S - HAsO_3^- + H_2O + H^+ \quad (11)$$

$$\equiv S - OH^- + HAsO_3^{2-} \rightarrow \equiv S - HAsO_3^{2-} + H_2O + H^+ \quad (12)$$

$$\equiv S - OH^- + As_3^{3-} \rightarrow S - AsO_3^{3-} + H_2O + H^+ \quad (13)$$

On the other hand, As(V) speciation revealed that at pH < 2, the neutral species H_3AsO_4 dominate the solution. Low uptake could be due to restricted interaction between the neutrally charged As(V) species and the positively charged adsorbent surface (Eq. 14). As the solution pH increases the negatively charged species such as $H_2AsO_4^-$, $HAsO_4^{2-}$ and AsO_4^{3-}. The dominance of this species at pH below the pHpzc enhances the adsorption of As(V) through attraction to positively charged surface followed by ion exchange and also through inner sphere complexation (Eq. 15) (Tiwari and Lee, 2012). At pH beyond the pHpzc, a decrease in As(V) could be attributed to repulsive forces between the abundant OH^- on the surface and negatively charged As(V) species (Eqs. (16) and (17)).

$$\equiv S - OH_2^+ + H_3AsO_4 \rightarrow \equiv S - OH - H_2AsO_3 + H_2O \quad (14)$$

$$\equiv S - OH_2^+ + H_2AsO_4^- \rightarrow \equiv S - H_2AsO_4^- + 2OH^- \quad (15)$$

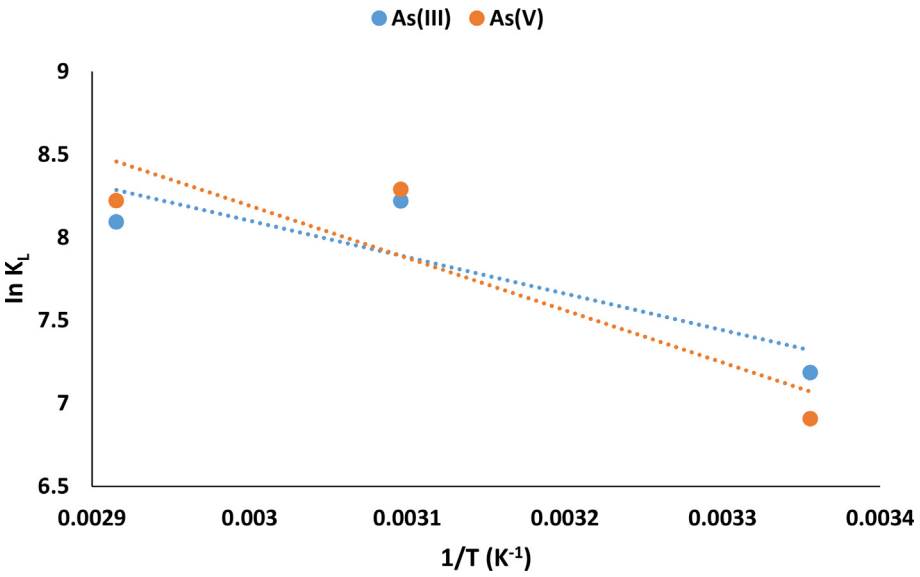

Fig. 11. Values of ln K_L as a function of reciprocal of adsorption temperature.

Table 6
Thermodynamic parameters.

	ΔG° (KJ/mol)	ΔH° (KJ/mol)	ΔS° (J/mol)
As(III)	298 K = -27.75	-18.24	18.7
	323 K = -32.85		
	343 K = -34.53		
As(V)	298 K = -27.06	-26.17	21.65
	323 K = -33.04		
	343 K = -34.89		

$$\equiv S - OH^- + HAs_4^{2-} \rightarrow \equiv S - HAsO_4^{2-} + H_2O + H^+ \quad (16)$$

$$\equiv S - OH^- + As_4^{3-} \rightarrow \equiv S - AsO_4^{3-} + H_2O + H^+ \quad (17)$$

3.12. Effect of co-existing ions

Groundwater naturally contains co-existing ions that could affect the adsorption of As(III) and As(V). To evaluate the effect of co-existing ions, As(III) and As(V) adsorption experiment was conducted in the presence of 10 mg/L of F^-, Cl^-. NO_3^-, CO_3^{2-}, SO_4^{2-}, Mg^{2+} and Ca^{2+}. The results are presented in Fig. 13. It is evident that the presence of F^-, Cl^-, NO_3^-, CO_3^{2-} and SO_4^{2-} inhabits the percentage As(III) and As(V) removal. This suggests that these anions compete with arsenic species leading to its reduced percentage of removal. Conversely, the presence of Mg^{2+} and Ca^{2+} increased the percentage of As(III) and As(V) removal. The percentage As(III) removal increased from 81.2% to 98% and 93.8% while that of As(V) increased from 86.6% to 98.2% and94.8% respectively in the presence of Mg^{2+} and Ca^{2+}. Similar results were reported by Qi et al. (2015) during the adsorption of As(III) and As(V) onto Fe–Mn binary oxide impregnated chitosan beads who cited that Mg^{2+} and Ca^{2+} enhances the positive charges and create more active sites on the surface of the adsorbent leading to higher sorption of As(III) and As(V) via attraction.

3.13. Regeneration and reuse of adsorbent

A sustainable and cost effective adsorbent for As(III)/As(V) removal from groundwater should be regenerated. To evaluate the regeneration potential of arsenic loaded SMK, five consecutive adsorption-desorption cycles were conducted using 0.1 M Na_2CO_3 as a regenerating agent. In Fig. 14 it is observed that the As(III)/As(V) removal efficiency decreased

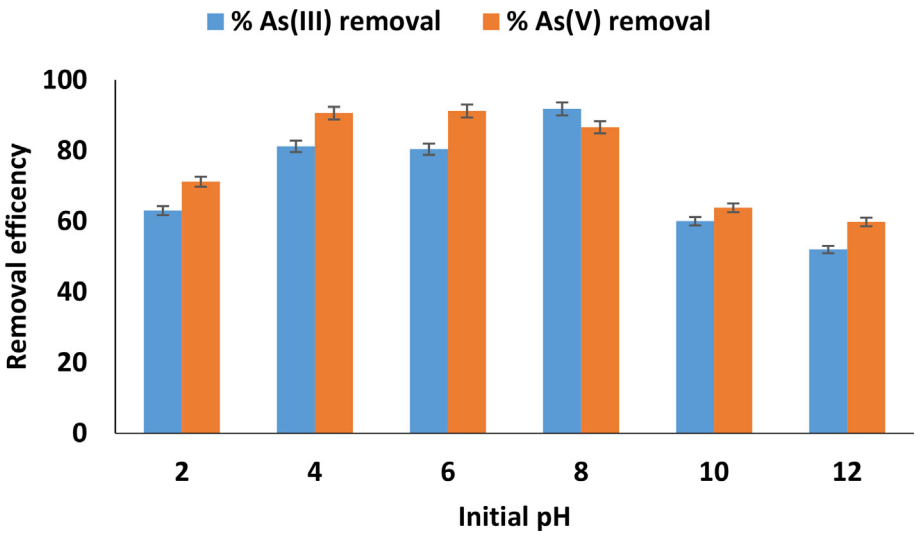

Fig. 12. Effect of pH onto As(III)/As(V) removal by SMK.

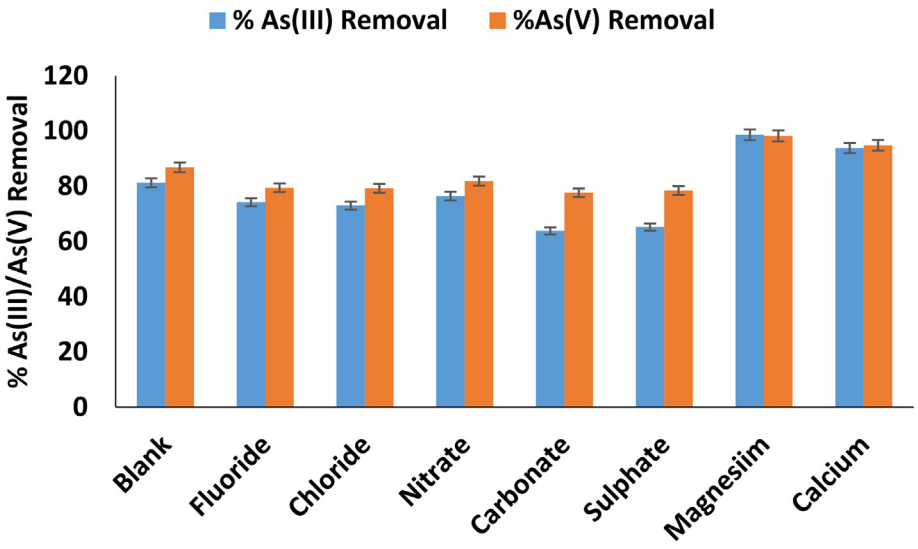

Fig. 13. Effect of co-existing ions during the adsorption of As(III) and As(V) by SMK.

with continuous regeneration from 95.8 and 97.6%, respectively achieved from the fresh sorbent to 54.1 and 62.3%, respectively at 5th cycle of reuse. Sahu et al. (2016) observed the same trend for arsenic removal using Ce–Fe bimetal metal oxides. The decrease in adsorption efficiency could be due to inadequate regeneration of the adsorbent's active sites.

3.14. Column experiment

Column test were conducted to evaluate the practical applicability of SMK in the arsenic removal from groundwater. Groundwater with physicochemical properties in Table 7 was spiked with groundwater to get a total arsenic concentration of 0.5 and 1.5 mg/L Fig. 15 presents the breakthrough curves obtained at different initial concentration. It is observed that increasing concentration of feed water decreases the breakthrough point (i.e. the point at which the As concentration in the effluent is equivalent to 0.01 mg/L (WHO guideline value)). This could be attributed to increasing driving force as the concentration increases leading to faster saturation of the adsorbent sites. At initial concentration of 0.5 mg/L, the throughput volume was 875 mL when the breakthrough point was reached ($C_e/C_o = 0.02$). Conversely, at initial concentration of 1.5 mg/L the breakthrough point ($C_e/C_o = 0.06$) was reached when the throughput volume (200 mL). The adsorption capacities at breakthrough point (q_B) and at exhaustion point (q_E) were found to be 0.38 and 1.23

Table 7
Physicochemical composition of groundwater at breakthrough point.

Parameter	Before treatment	Breakthrough point	WHO guideline (2017)
pH	8.7	6.98	5.0–9.7
As Total	0.5	0.01	0.01
F^-	5.4	0.98	1.5
Cl^-	31.59	22.1	<300
SO_4^{2-}	11.89	4.89	<500
NO_3	2.67	ND	50
PO_4^{3-}	1.3	ND	-
Mg	8.98	8.12	200
Na	70.36	69.12	200
Ca	10.87	8.12	200

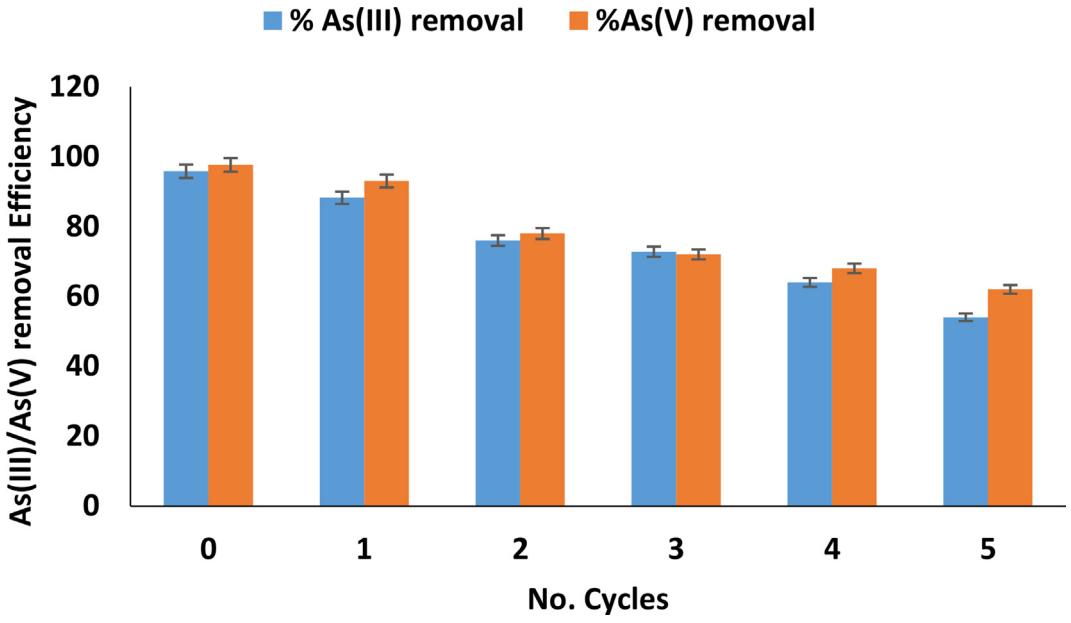

Fig. 14. As(III) and As(V) percentage of removal by SMK as a function of regeneration cycle.

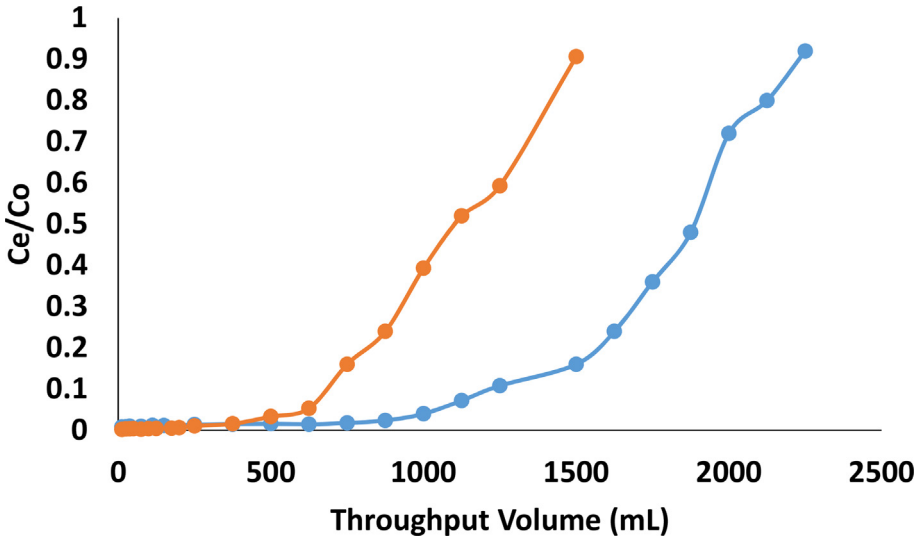

Fig. 15. Breakthrough curves for arsenic removal from spiked groundwater by SMK.

mg/g, respectively for 0.5 mg/L initial As concentration and 0.23 and 1.67 mg/g, respectively for 1.5 mg/L initial As concentration. It is interesting to note that at breakthrough point the physicochemical properties of the field water were improved (Table 7). The adsorbent exhaustion rate (AER) determined using Eq. (10) were found to be 5 g/L and 25 g/L for 0.5 mg/L and 1.5 mg/L, respectively.

$$AER = \frac{mass\ of\ the\ adsorbent\ (g)}{Breakthrough\ volume\ (L)} \quad (18)$$

The obtained results suggest that SMK produced in this study is a suitable adsorbent for arsenic removal from groundwater. In order to treat 20 L water containing arsenic concentration below 0.5 mg/L at a flow rate of 1.5 mL, an estimate of 0.15 kg of SMK will be required. Based on the results presented here, SMK synthesized in this study can be used for treatment of arsenic contaminated water.

Table 8
Comparison with other adsorbents.

Adsorbent	Experimental conditions	As(III) adsorption capacity (mg/g)	As(V) Adsorption capacity (mg/g)	Reference
Al-HDTMA sericite	Concentration = 1–20 mg/L, pH = 4.5, adsorbent dosage = 0.2 5/100 mL	0.33	0.85	Tiwari and Lee, 2012
Al-AMBA-sericite	Concentration = 1–20 mg/L, pH = 4.5, adsorbent dosage = 0.2 5/100 mL	0.43	0.51	Tiwari and Lee, 2012
Surfactant modified bentonite	Concentration = 0.2–60 mg/L; pH = 8.63; Adsorbent dosage, 1 g/100 mL	0.10	0.28	Su et al., 2011
HDTMA-Al-bentonite	Concentration = 2–18 mg/L; pH = 4.5; adsorbent dosage; 0.1 g/50 mL	2.47	8.93	Lee et al., 2015
HDTMA-Local-clay	Concentration = 2–18 mg/L; pH = 4.5; adsorbent dosage; 0.1 g/50 mL	2.18	4.1	Lee et al., 2015
HDTMA modified kaolin (SMK)	Concentration = 1–30 mg/L; pH = 6 ± 0.5; adsorbent dosage = 0.4 g/100 mL	2.3	2.88	Present study

3.15. Comparison with other adsorbents

In order to evaluate the competitiveness of SMK prepared in this study we compared the As(III) and As(V) adsorption capacity achieved in this study with the capacities reported in the literature. Table 8 shows the comparison with other adsorbent. From the table it is noticeable that SMK produced in this study is competitive over other adsorbent that have been reported in the literature and has a greater potential for use in arsenic removal.

4. Conclusions

In the present study, natural kaolin clay mineral was successfully modified through intercalation of HDTMA-Br surfactant onto the interlayers. The results from BET surface area showed that the modification of clay by HDTMA-Br reduced the total surface area from 18.61 to 3.39 m^2/g and increased the pore diameter increased from 9.53 to 20.41 nm. The synthesized adsorbent showed a maximum As(III) and As(V) adsorption capacities of 2.3 and 2.88 mg/g, respectively. The adsorption kinetics data for As(III) was described through PSO model while the data for As(V) was described by PFO model indicating that adsorption of As(III) was through chemisorption while the adsorption of As(V) was through physiosorption. Furthermore, the isotherm data for both As(III) and As(V) was best described by the Langmuir adsorption model indicating that adsorption occurred on a monolayered surface. Adsorption thermodynamics models revealed that during adsorption process As(III) and As(V) ions were distributed randomly and adsorption process was spontaneous and exothermic. The presence of anions such as F^-, Cl^-, NO_3^-, SO_4^{2-} and CO_3^{2-} decreased the adsorption efficiency while the presence of Ca^{2+} and Mg^{2+} increased the adsorption efficiency. The regeneration study revealed that SMK synthesized in this study can be used for up to 5 adsorption-desorption cycles. The results obtained from this present investigation showed that SMK is promising adsorbent for arsenic removal from groundwater.

Declarations

Author contribution statement

Rabelani Mudzielwana: Conceived and designed the experiments;

Performed the experiments; Analyzed and interpreted the data; Wrote the paper.

Wilson Gitari: Conceived and designed the experiments; Contributed reagents, materials, analysis tools or data; Wrote the paper.

Patrick Ndungu: Conceived and designed the experiments; Analyzed and interpreted the data.

Funding statement

This work was supported by National Research Foundation (NRF), South Africa, Sasol Inzalo Foundation (Saif) and University of Venda RPC grant Number: SES/17/ERM/03, TESPESKOM.

Competing interest statement

The authors declare no conflict of interest.

Additional information

No additional information is available for this paper.

References

Al-Othman, R. Ali., Naushad, M., 2012. Hexavalent chromium removal from aqueous medium by activated carbon prepared from peanut shell: adsorption kinetics, equilibrium and thermodynamic studies. Chem. Eng. J. 184, 238–247.

Arcibar-Orozco, J.A., Jouse, D.B., Rios-Hurtado, J.C., Rangel-Mandez, J.R., 2014. Influence of iron content, surface area and charge distribution in the arsenic removal by activated carbons. Chem. Eng. J. 249, 201–209.

Bentahar, Y., Hurel, C., Draoui, K., Khairoun, S., Marmier, N., 2016. Adsorptive properties of Moroccan clays for the removal of arsenic(V) from aqueous solution. Appl. Clay Sci. 119, 385–392.

Bhowmick, S., Chakraborty, S., Mondal, P., Renterghm, M.V., Berghe, S.V., Roman-Ross, G., Chatterjee, D., Iglesias, M., 2014. Montmorillonite-supported nanoscale zero-valent iron for removal of arsenic from aqueous solution: kinetics and mechanism. Chem. Eng. J. 243, 14–23.

Bretzler, A., Lalanne, F., Nikiema, J., Podgorski, J., Pfenninger, N., Berg, M., Schirmerm, M., 2017. Groundwater arsenic contamination in Burkina Faso, West Africa: predicting and verifying regions at risk. Sci. Total Environ. 584–585, 958–970.

Chutia, P., Kato, S., Kojima, T., Satokawa, S., 2009. Adsorption of As(V) on surfactant-modified natural zeolites. J. Hazard Mater. 162, 204–211.

Cui, J., Jing, C., Che, D., Zhang, J., Duan, S., 2015. Groundwater arsenic removal by coagulation using ferric(III) sulfate and polyferric sulfate: a comparative and mechanistic study. J. Environ. Sci. 32, 42–53.

Fatoki, O.S., Akinsoji, O.S., Ximba, B.J., Olujimi, O., Ayanda, O.S., 2013. Arsenic contamination: Africa the missing gap. Asian J. Chem. 52 (16), 9263–9268.

Firdaous, L., Fertin, B., Khelissa, O., Dhainaut, M., Nedjar, N., Chataigne, G., Ouhoud, L., Lutein, F., Dhulster, P., 2017. Adsorptive removal of polyphenols from an alfalfa white proteins concentrate: adsorbent screening, adsorption kinetics and equilibrium study. Separ. Purif. Technol. 178, 29–39.

Gitari, W.M., Ngulube, T., Masindi, V., Gumbo, R.J., 2015. Defluoridation of groundwater using Fe3+ modified bentonite clay: Optimization of adsorption conditions. Desalin. Water Treat. 53 (6), 1578–1590.

Gitari, W.M., Izuagie, A.A., Gumbo, J.R., 2017. Synthesis, characterization and batch assessment of groundwater fluoride removal capacity of tri-metal Mg/Ce/Mn oxide-modified diatomaceous earth. Arabian J Chem. In press.

Gupta, S.S., Bhattachryya, K.G., 2011. Kinetics of adsorption of metal ions on inorganic materials: a review. Adv Colloid Interface Sci. 162, 39–58.

Ho, Y.S., 2004. Citation review of lagergren kinetic rate equation on adsorption reactions. Scientometrics. 59 (1), 171–177.

Ho, Y.S., Wase, D.A.J., Forster, C.F., 1996. Kinetic studies of competitive heavy metal adsorption by sphagnum moss peat. Environ. Technol. 17 (1), 71–77.

Hong, J., Zhu, Z., Lu, H., Qiu, Y., 2004. Synthesis and arsenic adsorption performances of ferric-based layered double hydroxide with a-alanine intercalation. Chem. Eng. J. 252, 267–274.

Kang, M., Kawasaki, M., Tamada, S., Kamei, T., Magara, Y., 2000. Effects of pH on the removal of arsenic and antimony using reverse osmosis membranes. Desalination 131, 293–298.

Kempster, P.L., Silberbauer, M., Kuhn, A., 2007. Interpretation of drinking water quality guidelines- the case of arsenic. Water S.A. 33 (1), 95–100.

Lee, S.M., Lalmunsama, Thanhimngliana, Tiwari, D., 2015. Porous hybrid materials in the remediation of water contaminated with As(III) and As(V). Chem. Eng. J. 270, 496–507.

Lin, L., Qiu, W., Wang, D., Huang, Q., Song, Z., Chau, H.W., 2017. Arsenic removal in aqueous solution by a novel Fe-Mn modified biochar composite: characterization and mechanism. Ecotoxicol. Environ. Saf. 144, 514–521.

Lonappan, L., Rouissi, T., Brar, S.K., Verma, M., Suramphalli, R.Y., 2018. An insight into the adsorption of diclofenac on different biochars: mechanisms, surface chemistry, and thermodynamics. Bioresour. Technol. 249, 386–394.

McCann, C.M., Peacock, C.L., Edwards, K.A.H., Shrimpton, T., Gray, N.D., Johnson, K.L., 2018. In situ arsenic oxidation and sorption by a Fe-Mn binary oxide waste in soil. J. Hazard Mater. 342, 724–731.

Naushad, M., Ahmad, T., Al-Maswari, B., Alqadami, A.A., Alshehri, S.M., 2017. Nickel ferrite bearing nitrogen-doped mesoporous carbon as efficient adsorbent for the removal of highly toxic metal ion from aqueous medium. Chem. Eng. J. 330, 1351–1360.

Pakzadeh, B., Batista, J.R., 2011. Surface complexation modeling of the removal of arsenic from ion-exchange waste brines with ferric chloride. J. Hazard Mater. 188, 399–407.

Qi, J., Zhang, G., Li, H., 2015. Efficient removal of arsenic from water using a granular adsorbent: Fe–Mn binary oxide impregnated chitosan bead. Bioresour. Technol. 193, 243–249.

Reeve, P.J., Fallowfield, H.J., 2018. Natural and surfactant modified zeolites: a review of their applications for water remediation with a focus on surfactant desorption and toxicity towards microorganisms. J. Environ. Manag. 205, 253–261.

Ren, X., Zhang, Z., Lou, H., Hu, B., Dang, Z., Yang, C., Li, L., 2014. Adsorption of arsenic on modified montmorillonite. Appl. Clay Sci. 97–98, 17–23.

Sahu, U.K., Sahu, M.K., Mohapatra, S.S., Patel, R.K., 2016. Removal of As(V) from aqueous solution by Ce-Fe bimetal mixed oxide. J. Chem. Environ. Eng. 4, 2892–2899.

Saikia, R., Goswami, R., Bordoloi, N., Senapati, K.K., Pant, K.K., Kumar, M., Kataki, R., 2017. Removal of arsenic and fluoride from aqueous solution by biomass based activated biochar: optimization through response surface methodology. J. Chem. Environ. Eng. 5, 5528–5539.

Saleh, A.T., Sari, A., Tuzen, M., 2016. Chitosan-modified vermiculite for As(III) adsorption from aqueous solution: equilibrium, thermodynamic and kinetic studies. J. Mol. Liq. 219, 937–945.

Sari, A., Tuzen, M., 2009. Biosorption of As(III) and As(V) from aqueous solution by macrofungus (*Inonotus hispidus*) biomass: equilibrium and kinetic studies. J. Hazard Mater. 164, 1372–1378.

Sarkar, A., Paul, B., 2016. The global menace of arsenic and its conventional remediation – a critical review. Chemosphere 158, 37–49.

Smedley, P.L., Kinniburgh, D.G., 2002. A review of the source, behavior and distribution of arsenic in natural waters. Appl. Geochem. 17, 517–568.

Smith, A.H., Smith, M.M.H., 2004. Arsenic drinking water regulations in developing countries with extensive exposure. Toxicology 198, 39–44.

Su, J., Huang, H.G., Jin, X.Y., Lu, X.Q., Chen, Z.L., 2011. Synthesis, characterization and kinetic of a surfactant-modified bentonite used to remove As(III) and As(V) from aqueous solution. J. Hazard Mater. 185, 63–70.

Sun, K., Shi, Y., Chen, H., Wang, X., Li, Z., 2017. Extending surfactant-modified 2:1 clay minerals for the uptake and removal of diclofenac from water. J. Hazard Mater. 323A, 567–574.

Tiwari, D., Lee, S.M., 2012. Novel hybrid materials in the remediation of ground waters contaminated with As(III) and As(V). Chem. Eng. J. 204–206, 23–31.

Tran, H.N., You, S.J., Chao, H.P., 2016. Thermodynamic parameters of cadmium adsorption onto orange peel calculated from various methods: a comparison study. J. Chem. Environ. Eng. 4, 2671–2682.

Tran, H.N., You, S.J., Hosseini-Bandegharaei, A., Chao, H.P., 2017. Mistakes and inconsistencies regarding adsorption of contaminants from aqueous solutions: a critical review. Water Res. 120, 88–116.

Tuzen, M., Melek, E., Soylak, M., 2006. Celtek clay as sorbent for separation–preconcentration of metal ions from environmental samples. J. Hazard Mater. B136, 597–603.

Wang, J., Wang, T., Burken, J.G., Chusuei, C.C., Ban, H., Ladwig, K., Huang, C.P., 2008. Adsorption of arsenic (V) onto fly ash: a speciation-based approach. Chemosphere 72, 381–388.

Weber, W.J., Morris, J.C., 1963. Kinetics of adsorption on carbon from solution. J. Sanit. Eng. Div. 89 (2), 31–60.

World Health Organization, 2011. Guidelines for Drinking-Water Quality. Geneva: Switzerland, fourth ed.s.

Zhu, L., Zhu, R., 2007. Simultaneous sorption of organic compounds and phosphate to inorganic–organic bentonites from water. Separ. Purif. Technol. 54, 71–76.